Dressel, I., Scheck-Wenderoth, M., Cacace, M. (2017): Backward modelling of the subsidence evolution of the Colorado Basin, offshore Argentina and its relation to the evolution of the conjugate Orange Basin, offshore SW Africa. - *Tectonophysics*, *716*, pp. 168—181.

DOI: http://doi.org/10.1016/j.tecto.2016.08.007

Backward modelling of the subsidence evolution of the Colorado Basin, offshore Argentina and its relation to the evolution of the conjugate Orange Basin, offshore SW Africa

Ingo Dressel*[1,2], Magdalena Scheck-Wenderoth[1,2], Mauro Cacace[1]

1 German Research Centre for Geosciences – GFZ, Helmholtz Centre Potsdam, Germany

2 RWTH Aachen, Germany

*Corresponding author: dressel@gfz-potsdam.de, German Research Centre for Geosciences – GFZ, Helmholtz Centre Potsdam, Germany, Section 4.4, Telegrafenberg, 14473 Potsdam, Germany. Tel.: +49 331 288 1792 Fax: +49 331 288 1349

Keywords: Argentine passive continental margin, subsidence analysis, backstripping, Colorado Basin, Orange Basin

Abstract

In this study we focus on reconstructing the post-rift subsidence evolution of the Colorado Basin, offshore Argentina. We make use of detailed structural information about its present-day configuration of the sedimentary infill and the crystalline crust. This information is used as input in a backward modelling approach which relies on the assumption of local isostasy to reconstruct the amount of subsidence as induced by the sedimentary load through different time stages. We also attempt a quantification of the thermal effects on the subsidence as induced by the rifting, here included by following the uniform stretching model of lithosphere thinning and exponentially cooling through time. Based on the available information about the present-day

geological state of the system, our modelling results indicate a rather continuous post-rift subsidence for the Colorado Basin, and give no significant evidence of any noticeable uplift phase.

In a second stage, we compare the post-rift evolution of the Colorado Basin with the subsidence evolution as constrained for its conjugate SW African passive margin, the Orange Basin. Despite these two basins formed almost coevally and therefore in a similar large scale geodynamic context, their post-rift subsidence histories differ. Based on this result, we discuss causative tectonic processes likely to provide an explanation to the observed differences. We therefore conclude that it is most probable that additional tectonic components, other than the ridge-push from the spreading of the South Atlantic Ocean, are required to explain the observed differences in the subsidence of the two basins along the conjugate passive margins. Such additional tectonic components might be related to a dynamic mantle component in the form of either plume activity (Africa) or a subducting slab and the presence of an ongoing compressional stress system as revealed for different areas in South America.

1 Introduction

In the last decades, the passive continental margins of the South Atlantic have been the subject of a still increasing number of studies (e.g. Dupré et al., 2010; Hirsch et al., 2007, 2009; Jungslager, 1999; Katz and Mello, 2000; Maystrenko et al., 2013; Séranne and Anka, 2005). Efforts focus on detailed analysis of their sedimentary cover, their present-day architecture and configuration and tectonic history as based on geophysical (Autin et al., 2013, 2015; Franke et al., 2006; Gladczenko et al., 1997; Hinz et al., 1999; Loegering et al., 2013; Kuhlmann et al., 2010, 2011; Stewart et al, 2000), geochemical (Hartwig et al., 2012; Trumbull et al., 2007), sedimentological (Brown et al., 1995) or geodynamic (Braun et al., 2014; Colli et al., 2014; Flament et al., 2013;

Torsvik et al., 2009) evidences. The results from these studies have inspired more recent efforts aiming at investigating the details of the subsidence history of these basins, mainly published for the margins offshore SW Africa (Hirsch et al., 2010; Rouby et al., 2013; Dressel et al., 2015, 2016) and rarely made at the conjugate margin of SE South America (Sachse et al., 2015). So far, attempts to compare the evolution of the two South Atlantic margins (in terms of major controlling factors on hydrocarbon generation) have only been made by Marcano et al. (2013).

In addition, previous studies relied on two-dimensional forward numerical models of the large-scale rift dynamics (Burov et al., 2007; Burov and Cloething, 2010; Huismans and Beaumont, 2011, 2014; Brune et al., 2014) and even three-dimensional forward approaches (Allken et al., 2012; Le Pourhiet et al., 2012, Brune et al., 2013; Brune 2014; Koopmann et al., 2014; Liao and Gerya, 2015). These studies have provided a significant advance in the current understanding of continental rifting dynamics, and have been beneficial to explain first order differences in the basic configuration of the margins. The main limitation of these approaches is that they are based on a highly simplified geometry of the lithosphere, where sediments are either not considered or integrated as a passive load acting on the plate. These aspects hinder the use of forward models to reconcile the details of the sedimentary infill as constrained in such basins.

In this study, we focus on reconstructing the post-rift subsidence of the Colorado Basin, offshore Argentina (Figure 1) based on present-day observations. Therefore, we rely on data available on the geology (i.e., crustal configuration and sedimentary succession) that has been summarized in an integrative detailed 3D model of the present-day configuration of the Colorado Basin offshore Argentina (Autin et al., 2013; 2015). The preserved sediment thicknesses are used in a backward modelling approach to derive the subsidence history and to quantify past vertical movements along the passive continental margin of Argentina since the time after the breakup of the southern segment of the South Atlantic Ocean. In our study, we do not attempt any modelling

reconstruction of the rifting stage initiating the basin, but we rather focus on the post-rift subsidence evolution. In this regard, our aim is to make use of the detailed dataset available to quantify the maximum amount of subsidence that is induced by the sediments and, additionally, by the thermal cooling of the lithosphere. To quantify the latter we rely on the assumption of uniform stretching (McKenzie, 1978) as a simple, though effective way to parameterize the amount of additional thermal subsidence throughout the post-rift evolution. This study resorts to the uniform stretching assumption despite and aware of the limitation inherent in the method (e.g., ignoring radiogenic heat production and thermal blanketing by the sediments; assuming a fixed temperature at the depth of the lithosphere). The main reason on adopting a simple, one dimensional analytical solution is that it does not require a wide spectrum of parameters, which are usually difficult to constrain, if not disputable, as more sophisticated solutions to the thermal problem do. In addition, our study does not attempt any modelling of the complex and non-linear physics initiating the subsidence. It rather makes a systematic use of available geological data to derive information about the complex history of these margins, in a way that might help identifying most likely causative tectonic processes. These geological data constrain the preserved thickness of sediments and thus the amount of subsidence induced by sedimentary loading. In addition, we consider it justifiable to use a simplified kinematic representation of the thermal evolution of the system, by taking at the same time all limitations behind our choice into account while discussing the results obtained from the investigation. From the above discussion it follows that the computed subsidence should be considered as a maximum value (upper threshold; Dressel et al., 2016).

In a second stage, the results obtained for the Colorado Basin are compared to a previous study where, by following a similar work-flow, we did attempt a reconstruction of the subsidence at the conjugate Orange Basin, offshore SW Africa (Dressel et al., 2015). The main outcome of the

comparison is that, although these margins evolve simultaneously after the breakup of the South Atlantic Ocean (~125 Ma),they have been characterized by a different subsidence evolution throughout their post-rift phases. Therefore, the results from this comparison opens a discussion about possible causative tectonic processes responsible for the evolution of these two basins as detailed in the last part of this manuscript by also taking their geological context into account.

2 Geological setting and dataset

It has been long recognized that the origin of the volcanic passive margins of SE America and SW Africa was coeval and resulted from the breakup of Gondwana during Early Cretaceous (Austin and Uchupi, 1982; Rabinowitz and Labrecque, 1979; Sibuet et al., 1984). Supercontinental breakup was followed by the opening of the South Atlantic Ocean showing a preferential northward propagation which was accompanied by extensive volcanism and the emplacement of lower crustal bodies and seaward dipping reflectors within the southern segment of the South Atlantic Ocean (Franke et al., 2007, 2010; Hinz et al., 1999; Schnabel et al., 2008).

After breakup had ceased (around approximately 125 Ma), the Argentine margin underwent a phase of long post-rift subsidence marked by lithospheric cooling of the rift-related thermal anomaly and consequent sediment accumulation. At present, the Colorado Basin shows two major domains in style of deformation (Autin et al., 2013, 2015). While the western part of the basin is underlain by a NW-SE striking depocentre, its distal segment has a NE-SW oriented axis (Figure 2). According to previous studies (Autin et al., 2015; Dominguez et al., 2011; Franke et al., 2006) four segments (western-, central-, eastern- and distal segment; Figure 2) can be further distinguished as associated to major transfer zones proposed to represent strike-slip-like structures.

The post-rift subsidence created accommodation space for a total sediment fill of up to 8,000 m in the main depocentres, with a sediment supply mainly consisting of siliciclastic rocks as well as subordinate gypsum, limestones and marine shales (Autin et al., 2013 and references therein).

For our investigation, we make use of an existing 3D structural crustal-scale model of the entire Colorado Basin (Autin et al., 2013; 2015). The model has an extension of 350 x 850 km in N-S and W-E direction, respectively. It distinguishes a water column unit according to the present-day bathymetry, and seven post-rift units, which from top to bottom are listed as followed: Shallow, 0-27 Ma; Caotico, 27-35 Ma; Elvira, 35-55 Ma; Pedro Ludro, 55-70 Ma; Colorado III, 70-85 Ma; Colorado II, 85-100 Ma; Colorado I, 100-125 Ma (see Figure 3a-g for the respective thickness maps). In general, the isopach maps indicate a major depocentre in the west, close to the Argentine coast, as well as in the east, along the distal margin. Older units (125 Ma to 70 Ma), such as Colorado I, Colorado II and Colorado III are marked by larger thicknesses while younger sedimentary units (70 Ma to 25 Ma) become thinner (Pedro Luro, Elvira and Caotico) with a final thickening of the Shallow unit (25 Ma to present-day).

As mentioned above, two major depocentres are characteristic for the Colorado Basin. However, they vary in accommodation space. Figure 4 illustrates the stratigraphy of two synthetic wells with thicknesses according to the published structural model by Autin et al. (2013, 2015). The location of the synthetic wells is chosen with respect to the major depocentres. Apart from the Elvira unit and Colorado II unit that are thicker in the western segment, larger sediment thicknesses are found in the distal segment.

According to the original model, these seven post-rift units overly a syn-rift sedimentary unit resting upon a crystalline crustal basement. Autin et al. (2015) differentiated the crust into

different domains in terms of bulk density including seaward-dipping reflectors (SDRs), a crystalline crust and lower crustal bodies (LCBs). These are schematically depicted in Figure 5, which shows a profile across the Colorado Basin highlighting the distribution of the sediments, the location of the different crustal bodies in the crystalline crust as well as the depth to the Moho. In addition, Figure 5 shows the increased stretching of the crust in the direction of the distal segment (towards the east). A crystalline crustal thickness of ~23,000 m is representative for the western segment, whereas the distal segment has a crystalline crustal thickness of ~15,500 m.

For the aim of this study, investigating the post-rift phase, we assume the SDRs and LCBs to have been emplaced before or coeval to rifting so that these bodies do not thermally affect the post-rift phase. This assumption is in agreement with suggestions by Autin et al. (2015) for the Colorado Basin and Thybo and Artemieva (2013) for other passive margin settings. Although the thermal subsidence is not affected by the emplacement of the SDRs and LCBs, the amount of load induced subsidence varies as the isostatic feedback from the previous emplacement of the crustal bodies onto the post-rift subsidence evolution of the basin will affect the subsidence analysis in that denser or lighter material would affect the isostatic rebound and therefore the amount of subsidence. Consequently, we parameterize the crustal density by calculating a laterally varying density for the crystalline crust. Therefore, we integrate in our calculations a single crustal domain extending beneath the base of the syn-rift sediments down to the Moho boundary (Figure 5) and calculate the lateral varying density of area. This was done by assuming local isostatic equilibrium at the Moho. Figure 6 shows the thickness of the present-day crystalline crust and the corresponding laterally varying density (i.e., including areas of denser material such as where SDRs and LCBs emplaced pre-breakup). Figure 6a illustrates how the crust is thinned in eastern direction. The thinnest crust is obtained along the COB (less than

~15,000 m), whereas the thickest crust is obtained in the north and the south of the research area (~35,000 m).

According to the calculated laterally varying density distribution (Figure 6b), there is a strong spatial correlation between the areas of higher densities and the occurrence of SDRs and LCBs according to Autin et al. (2015). Higher densities are obtained within the central segment of the basin as well as along the distal margin. Autin et al. (2015) differentiate between areas of LCB emplacement as depocentre-related LCBs, distal margin-related LCBs and SDR-related LCBs. Comparing their map of LCB thickness with the density distribution illustrated in the present study (Figure 6b) shows a strong spatial correlation in location of LCBs and areas with higher density. Furthermore, the same is valid for the map of SDR thickness (by Autin et al., 2015), showing a NE-SW striking trend of SDRs which is in agreement to the higher densities along the COB presented in Figure 6b. This correlation allows using the calculated lateral varying density for the backward modelling approach.

3 Method

We use a multi 1D backward modelling approach based on present-day observations to quantify the subsidence evolution during the entire post-rift stage (from approximately 125 Ma until the present-day) of the Colorado Basin. Information about the structural configuration of the Colorado Basin is taken from the 3D structural model by Autin et al., (2013; 2015).

Accordingly, after removal (i.e., backstripping) of each unit we back-calculate the amount of isostatic readjustment of the column following the concept of local Airy isostasy (Airy, 1855). Our calculation takes decompaction of the remaining sediments according to unloading into account and is parameterized following Athy's exponential porosity-depth relation (Athy, 1930)

by considering an additional porosity-load dependence (Scheck et al., 2003). Table 1 lists all properties adopted for each individual sedimentary unit (Autin et al., 2015) as well as the age subdivision after Autin et al. (2013) with modifications on the most recent timescale by Cohen et al. (2013).

The additional load from the water column is here considered only at the beginning of our calculation. There are two main reasons behind our assumption: First, the water depth was shallower during the past because load (due to sediments) and thermal subsidence (due to relaxation of the lithosphere) affected the margin during the post-rift phase. For this reason, the water depth at the present-day represents the maximum water depth during the entire post-rift phase. Second, in our study area the average water depth at the present-day is only less than 150 m beneath the areas of the major deposition. From this it follows that the water column would only yield about 50 m of isostatic rebound, which is negligible when compared to the total post-rift sediment thickness of about 8,000 m yielding about 6,000 m of isostatic rebound on average.

Successive removal of the sedimentary units yields the amount of subsidence as induced by the deposition of each sedimentary unit (considered here as instantaneous) and a final backstripped surface as a result.

Though simplistic, 1D backward in time modelling, assuming local isostatic readjustment, has the particular advantage that it does not require the definition of the past rheology of the lithosphere which is needed for a flexural modelling approach and difficult to constrain. Indeed, estimating the rheology of the lithosphere during its past evolution meets uncertainties that likely will affect the results of the modelling in a non-deterministic way. To avoid any speculative determination, we here decide to rely on available data and make use of local isostasy and being aware of the limitations associated with our approach. In this regard, the reader should take in mind that the obtained results, express in terms of subsidence curves, will represent an upper value with respect

to the subsidence expected to have occurred during the evolution of the passive margin (Dressel et al., 2016).

As common to all backstripping approaches, it is not possible to take into account the additional effects of lithosphere cooling during the sediment deposition and resulting thermal subsidence. A study by Loegering et al. (2013) emphasized the role of this additional subsidence component related to conductive cooling of the lithosphere to explain the post-rift thermal subsidence within the Colorado Basin. In an attempt to correct the backstripped surface for lithospheric cooling, we calculate the amount of thermal subsidence separately by following the uniform stretching model (McKenzie, 1978). As discussed in the introduction, our workflow comes with some limitations mainly related to the validity of the uniform stretching model for real case passive margin settings. Indeed, it might be likely that rifting was not instantaneous but rather consisting of multiple rifting stages of finite duration, and that the sediments accommodated on a relaxing lithosphere of finite strength. However, insufficient information about input parameters to constrain the details of the rifting dynamics as well as the internal rheological configuration of the entire plate hindered any detailed quantification of such processes. Therefore, we decide to use a simple, analytical approach, without attempting any detailed reconstruction of the rifting phase. Furthermore, the reason for relying on a uniform stretching model to initialize and parameterize thermal cooling of the lithosphere stems from its simplicity to describe the model configuration by means of a dimensionless parameter, which is the β-factor. We have inferred the β-factor from the ratio between the thickness of the initial (i.e. un-stretched) and present-day crust affected by stretching (illustrated in Figure 8h). As the aim of this study is not to solely investigate the subsidence evolution of the Colorado Basin but also to compare this to the subsidence evolution of the Orange Basin on the conjugate margin offshore SW Africa, we assume the initial crustal thickness to be the same along both margins. Consequently, for a

consistent comparison between the conjugate margins of SE South America and SW Africa, the reference value for the un-stretched crust has been set equal to the one adopted in our previous study on the Orange Basin (Dressel et al., 2015).

The obtained thermal subsidence is used to correct the backstripped surfaces determined from the backstripping methods for each time interval considered, according to the differentiation listed in Table 1, and to restore paleobathymetries. Exemplarily, the paleobathymetry at 25 Ma is reconstructed by backstripping the water column and the Shallow unit with the result of a backstripped surface at 25 Ma, the top of the Caotico unit. This surface is then corrected for the amount of thermal subsidence calculated for the time interval between 0 Ma and 25 Ma. Following this procedure, the remaining seven paleobathymetries are obtained, always considering the thermal subsidence between 0 Ma and the respective stratigraphic unit.

4 Results

4.1 Results – Load induced subsidence

Figure 7 (a to g) shows the amount of load induced subsidence for the seven post-rift units. The largest amounts of subsidence occur during the early stages in the post-rift evolution, that is, from 125 Ma and 70 Ma. Subsidence during the last 70 Ma of the evolution of the basin is considerably less due to the deposition of smaller amounts of sediments during this time window.

A detailed analysis of the subsidence, induced by each sedimentary unit, reads as follows:

The deposition of the Colorado I unit induces about 1,300 m of subsidence in the distal part, and about 1,700 m in the central part and only a minor subsidence in the western part (about 700 m). Although deposition of the Colorado II unit lasts only for 8 Ma, the induced subsidence is comparable with the one determined for Colorado I with about 1,500 m in the distal to central part and about 1,100 m in the western part. Similar to Colorado II, Colorado III induces up to

1,700 m of load in the central to distal area and about 1,000 m in the western part. By contrast, the Pedro Luro unit contributes significantly less to the load induced subsidence with 580 m in the distal part, 240 m in the central part and 160 m in the western area of the Colorado Basin. The Elvira unit has its largest sediment thickness close to the COB. Accordingly, an amount of about 1,000 m of load induced subsidence is obtained in this local area while the central and western area of the Colorado Basin are characterized by about 200 m and 100 m of load induced subsidence, respectively. Although the Caotico unit deposited almost uniformly beneath the entire Colorado Basin it is also characterized by a relative small thickness when compared to the other sedimentary units. Therefore, we also obtain a minor amount of load induced subsidence of about 480 m in the distal part that decreases in westward direction to about 240 m in the central part and increases again up to 360 m in the western segment. Finally, the Shallow unit thickens again. For this reason, the amount of load induced subsidence is about 1,300 m in the central part and about 700 m in the western part.

4.2 Results – Thermal subsidence

Figure 8 (a to g) illustrates the amount of thermal subsidence as determined at the end of each of the seven post-rift phases. Following the uniform stretching model (McKenzie, 1978), the amount of thermal subsidence exponentially decays with time. This trend is generally also observed in our subsidence maps. Indeed, the amount of thermal subsidence is the largest during the early stages, that is, between 125 Ma and 70 Ma and significantly drops during the last 70 Ma. Not surprisingly, spatial variations in thermal subsidence strongly reflect variations in the β-factor considered (Figure 8 h). Therefore, we obtain the largest amount in thermal subsidence along the COB where stretching is highest as well as in the distal to central area where the stretching factor

ranges between 1.5 and 3. In westward direction the amount of stretching and therefore the amount of thermal subsidence decreases.

Furthermore, magnitudes of thermal subsidence also linearly depend on the time interval considered to calculate them. Shorter time-periods have a relatively smaller net amount of thermal subsidence when compared to larger time windows. According to the temporal resolution of our model and the respective duration of the deposition of the individual sedimentary units, the individual amounts of thermal subsidence can be described as follows:

After the first 27 Ma of the post-rift phase (deposition of Colorado I; 125 Ma to 98 Ma), higher amounts of thermal subsidence (approx. 1,050 m) are found across the COB and up to 950 m in the distal area. Subsidence decreases while moving inward the basin to values of approximately 780 m in the central and 680 m in the western area. During the second post-rift interval (Colorado II; 98 Ma to 90 Ma), the amount of thermal subsidence is relatively small (compared to the previous stage) with only 175 m at the COB decreasing to 150 m in the distal part and 125 m in the central part. These lower values are related to the short duration of this stage lasting approximately 8 Ma. During the deposition of the Colorado III unit (90 Ma to 70 Ma), the amount of calculated thermal subsidence increases with respect to the previous stage, from about 280 m at the COB to about 220 m in the western area with 210 m in between. The time interval between 70 Ma and 55 Ma (Pedro Luro unit emplacement) is characterized by about 120 m of thermal subsidence along the COB as well as in the distal area. A relative drop in thermal subsidence (to about 90 m) is obtained for the central part while for the western part only 72 m of thermal subsidence are predicted. From 55 Ma onward, the lithosphere is almost re-equilibrated as shown by only minor amounts of thermal subsidence. During 55 Ma to 40 Ma (Elvira unit emplacement) the amount of thermal subsidence ranges between 75 m in the distal part and 50 m in the western part. Likewise, the next younger time interval encompassing the deposition of the

Caotico unit (40 Ma to 25 Ma) is characterized by an amount of thermal subsidence less than 45 m along the COB and about 30 m in the western part with 38 m in between. Finally, the last 25 Ma (Shallow unit emplacement; 25 Ma to 0 Ma) show almost no variations compared to the time interval before. Accordingly, we obtain 40 m of thermal subsidence along the COB, 36 m in the distal part, 31 m in the central part and only 27 m in the western part.

4.3 Results – Paleobathymetries

In an attempt to discuss the net effect of thermal subsidence by lithospheric cooling and load induced subsidence from sedimentation, we discuss in the following the obtained paleobathymetries for each of the seven post-rift stages (Figure 9).

By inspecting these figures, it is evident that the Colorado Basin has been affected by continuous subsidence from breakup to the present-day as the water depth shallows after correcting for the load induced subsidence and thermal subsidence.

Going backward in time, the restored paleobathymetry at the start of deposition of the Shallow unit (top of the Caotico unit; 25 Ma) displays water depths less than 200 meter below sea level (m.b.s.l) in the western and central part of the Colorado Basin that deepens to about 280 m.b.s.l in the north and 480 m.b.s.l in the south. A rapid deepening to about 700 m.b.s.l occurs at about 100,000 m westward of the COB (to which we refer as distal margin in the following). The area along the COB is characterized by about 2,800 m.b.s.l. At 40 Ma (top of Elvira unit), the paleobathymetry is less than 300 m.b.s.l in the western and central segment with larger depths of up to 550 m.b.s.l in the south and 400 m.b.s.l in the north. Towards the Atlantic Ocean, we obtain a paleobathymetry ranging from 800 m.b.s.l along the distal margin up to a maximum of 2,800 m.b.s.l at the COB. The paleobathymetry at the top of the Pedro Luro unit (55 Ma) does not show any sensible changes with respect to the one discussed previously, mainly because of the

presence of thin sediments which have deposited during this time window. The restored paleobathymetry at the start of the deposition of the Pedro Luro unit (top of the Colorado III unit; 70 Ma) shows values as low as 150 m.b.s.l in the central- and western part, increasing gradually to 400 m.b.s.l in the north, 580 m.b.s.l in the south and up to a maximum of 2,800 m.b.s.l at the COB. Removing Colorado III unit and correcting for the respective thermal subsidence yields the top Colorado II surface (90 Ma). We obtain about 500 m.b.s.l of paleobathymetry in some central areas with larger values of 700 m.b.s.l in the southwest. A depth-range of 1,000 m.b.s.l to 2,800 m.b.s.l is obtained at the distal margin. At the top of the Colorado I unit (98 Ma) the paleobathymetry shows values of 900 m.b.s.l in the central and western part with an exception of 300 m.b.s.l in between the western and central segment. By contrast, the north and the south is marked by about 500 m.b.s.l of depth. The distal part has a paleobathymetry of about 1,100 m.b.s.l and up to 2,600 m.b.s.l at the COB. Finally, we obtain the last paleobathymetry at 125 Ma which is the top of the syn-rift unit. The resulting paleobathymetric map has an overall paleobathymetry of 750 m.b.s.l in the western and central part and down to 1,700 m.b.s.l at the COB. In addition, some local areas of positive paleotopography up to 100 m.a.sl. in the north close the present-day coast line are characteristic for this time.

5 Discussion

As discussed above, major changes in the depth of the paleobathymetries occur during early times after the breakup (from 125-70 Ma) while only minor changes are depicted for the remaining 70 Ma up to present-day. This latter time period is also characterized by deposition of smaller amounts of sediments (Shallow, Caotico, Elvira and Pedro Luro units; Figure 7) than those during the early post-rift stage (Colorado III, Colorado II and Colorado I units; Figure 7). Besides, the oldest (before 70 Ma) units were mainly deposited beneath the central and eastern

part, whereas the younger units (70 Ma to 0 Ma) were deposited more towards the eastern part, thus marking the major depocentres as presently observed within the basin area (Figure 2).

Additionally, because the lithosphere is almost isostatically equilibrated, these latest stages have also the smallest amounts of thermal subsidence (Figure 8). Therefore, we can identify a two stage subsidence evolution for the Colorado Basin on first order effects, characterized by higher vertical movement during the first 55 Ma after breakup and only relatively minor ones occurring during the remaining 70 Ma, during which time period also the paleo-water depths did not change significantly.

To discuss the evolution of the subsidence constrained for the Colorado Basin and to carry out a comparison with the reconstructed subsidence at the conjugate margin offshore SW Africa, we plot one dimensional subsidence profiles as extracted from the two synthetic wells beneath the Colorado Basin (stratigraphy in Figure 4, see Figure 1 for location): one chosen as representative for the western and one from the eastern segment (Figure 10). In addition, the subsidence curves derived from a previous study, focused on the Orange Basin (Dressel et al., 2015), are also plotted to facilitate our discussion.

The 1D profiles are representative of a trend considered typical of a passive margin setting (Bott, 1992). According to Figure 10, the western and eastern areas of the Colorado Basin vary in the amount of total subsidence in that the eastern segment experienced more subsidence than the western segment, giving a final difference of approximately 2,500 m of subsidence at present. The difference can be interpreted as being partially the result of larger amounts of stretching in the eastern segment ($\beta = 2.52$) than in the western segment ($\beta = 1.73$). However, the magnitudes of variations in the stretching factors alone are insufficient to explain the amount of difference in the calculated total subsidence. Most likely, variations in the sedimentation (rates and supply, i.e.

load induced subsidence) are to be called for in order to reconcile these observations. The amount of load induced subsidence can be calculated from Figure 10 as the area between the thermal and total subsidence curves. By calculating the individual amounts of load induced subsidence at each time interval, no general relationship between the two segments can be discriminated. Accordingly, we obtain a larger load induced subsidence in the western segment for the time interval between 40 Ma to 25 Ma (deposition of the Caotico unit) and between 55 Ma to 40 Ma (deposition of the Elvira unit) of about 475 m and 330 m, respectively. For the other time intervals, the eastern segment has larger amounts of load induced subsidence. These aspects strongly suggest that although the Colorado Basin has been characterized by continuous subsidence since breakup, its post-rift history is likely the result of several components (e.g., change in depositional environment) which acted at different temporal and spatial scales. During the time interval of 98 Ma to 90 Ma, the amount of load induced subsidence is almost the same in the western and eastern segment.

Comparing the subsidence curves as described before with a one dimensional profile extracted for the conjugate Orange Basin, offshore SW Africa (Dressel et al., 2015) reveals differences between the two margins. The amount of thermal subsidence, determined for the Orange Basin, is comparable with the Argentine margin, which is plausible given the fact that similar stretching conditions during breakup occurred at both settings. While the stretching factor for the Colorado Basin is 1.73 (western segment) and 2.52 (eastern segment), respectively, the Orange Basin thermal subsidence curve is calculated using a β of 2.0 (Figure 10). Therefore, it represents an average between the thermal subsidence curves of the Colorado Basin. By contrast, the amount of total subsidence significantly varies between the Orange and the Colorado Basin. The Orange Basin experienced its largest total subsidence during the Cretaceous, while the eastern segment of

the Colorado Basin experienced also a larger total subsidence during Cenozoic times. At about 67 Ma the total subsidence curves of the Orange Basin and the eastern Colorado Basin cross each other with the result of more total subsidence within the western Colorado Basin than in the Orange Basin (a difference of up to 1,403 m at the present-day). As the amount of thermal subsidence is within the same order of magnitude, the reason for the varying total subsidence relates to different amounts of sediment supply in the two basins, higher for the Colorado than for the Orange Basin. This is in agreement with the sedimentation rates suggested by Loegering et al. (2013). However, while a change in sediment supply could have surely played a role in shaping the overall subsidence history of the two basins, it is also possible that other processes might have come into play as well. In this regard, seismic profiles across the Orange Basin show several unconformities that are partially interpreted as erosional truncation horizons (Brown et al. 1995; Hirsch et al, 2010; Kuhlmann, et al. 2010; Paton et al., 2007). In addition, Hirsch et al. (2010) evaluated that the best fit between modeled and observed vitrinite reflectance data can be achieved only by considering an erosion of about 1,000 m. Furthermore, erosional events are also in agreement with investigations onshore South Africa by Braun et al. (2014). These authors relate the erosion of the South African plateau to a major uplift episode during the Late Cretaceous. Consequently, it is most probable that differences between the subsidence curves for the Colorado Basin and the Orange Basin can, at least partly, result from extensive post-depositional erosion of the sediments in the Orange Basin. These erosional processes may have been related to tectonic uplift, processes that did not affect the South American conjugate margin. If this was the case, the question that remains is which mechanisms could have caused such asymmetric uplift. Furthermore, it remains open which tectonic force has been the cause of this uplift and during which time in the evolution of the two settings it was acting. In this sense, a possibility would be the ridge push due to the spreading of the South Atlantic Ocean (Japsen et

al., 2012). Alternatively, the detected uplift could be the surface expression of a deep mantle mechanism (Nyblade and Robinson, 1994), an aspect to which there is still an open debate. Some studies identified plume activity beneath the African continent as a possible force triggering the uplift and leading to erosion of the younger strata (Moucha and Forte, 2011; Colli et al., 2014). Regarding the African continent, results from of Dressel et al. (2015) also indicate post-rift seafloor uplift along the SW African margin interpreted as the result of either a deep mantle mechanism or of another tectonic force, possibly related to lower crustal flow.

Winterbourne et al. (2014) analyzed and quantified residual topographies for the oceanic domain. This residual topography is often linked to dynamic topography and therefore to fluid-like circulation within the sub lithospheric convective mantle. The study by Winterbourne et al. (2014), constrained a negative residual topography of about -1,000 m offshore Argentina. By contrast, the residual topography offshore SW Africa has been quantified to an amount of about 700 m above sea level. According to the restored paleobathymetries of this study, there is no indication for seafloor uplift within the Colorado Basin while reconstructed paleobathymetries strongly indicate seafloor uplift of about 1,000 m above sea level for the Orange Basin (Dressel et al., 2015). Although based on a different method, the results obtained from the study well correlate, both in terms of determination style and overall magnitude of vertical displacement, with those obtained and discussed by Winterbourne et al. 82014), an aspect that we use to substantiate our hypothesis of mantle dynamics as causative mechanism for the observed differences in the dynamic evolution of the two conjugate margins (see also the following discussion).

Regional uplift in the Colorado Basin area during the Upper Cretaceous and Paleocene/Eocene has also been discussed by Autin et al. (2013). However, this study offers no explanation for these events. The results from the study by Cobbold et al. (2007) indicate a regional

compressional stress state within South America since the Cretaceous (and possibly still ongoing) as induced by the subduction of the Nazca Plate beneath the South American plate and ridge push forces from ongoing opening of the South Atlantic. However, their discussions rather focus on the Santos Basin, north of the Colorado Basin offshore SE Brazil. Therefore, their results cannot be directly compared to the Colorado Basin. Furthermore, Sachse et al. (2015) reported uplift in the Austral Basin, located on- and offshore South America and the Malvinas Basin, both 1,200 km south of the Colorado Basin. Therefore, it is likewise difficult to compare the evolution of those basins with the Colorado Basin. For the research area of the present study, Demoulin et al. (2005) linked Cretaceous sediments within the Colorado Basin to erosion in the Ventana massif (NW of the Colorado Basin, onshore South America). They concluded from their morphogenetic model that the Ventana massif underwent two uplift phases that are in accordance with the observed increase in sedimentation rates in the Colorado Basin. They interpreted these uplift episodes as caused by the South Atlantic opening during the Cretaceous and a Neogene reactivation of structures in the foreland of the Andes.

In the light of the results of all the previous studies as described above, obtained differences in the subsidence evolution of the conjugate Argentine and SW African margins give evidence that ridge push forces related to the dynamics of the South Atlantic are to be considered at most of secondary relevance in affecting the evolution of the South Atlantic margins. Therefore, we agree with other studies in assuming mantle dynamics as causative for the recorded uplift across SW Africa (Braun et al., 2014; Colli et al., 2014; Gurnis et al., 2000; Lithgow-Bertelloni and Silver, 1998; Ritsema et al., 1999; Dressel et al., 2015). This is in agreement with the presence of erosional unconformities within the stratigraphic record of the Orange Basin (Hirsch et al., 2010; Kuhlmann et al., 2010) and with the main conclusions of Loegering et al. (2013) demonstrating

no evidence for any significant erosion (even as low as few tens of meters) in the Colorado Basin since the breakup of the South Atlantic.

6 Conclusions

The subsidence analysis of the Colorado Basin using present-day information about the configuration of the sediments and the crystalline crust allows quantifying the amount of load induced subsidence as well as the amount of the thermal subsidence for seven time intervals during the post-rift phase. This information is used to reconstruct paleobathymetries of the Colorado Basin that indicate continuous subsidence through the entire post-rift phase.

Comparing the paleobathymetries restored for the Argentine margin with those of the conjugate margin offshore SW Africa reveals significant differences of the subsidence history on both margins. In contrast to the Argentine margin paleobathymetries, those at the SW African margin indicate intermittent periods of elevations above sea level that might be related to uplift and erosion.

Discussing these insights points out that additional tectonic forces, other than ridge-push due to the spreading of the South Atlantic Ocean, are needed to explain the differences between the reconstructed subsidence evolution of the Orange Basin and Colorado Basin. If ridge-push is the primary mechanism responsible for seafloor uplift its consequence should be evident at the Argentine margin to the same extent as at the conjugate SW African margin. For this reason, the comparison between the subsidence history of the Colorado Basin and the Orange Basin points to a deep mantle mechanism that is responsible for the reconstructed seafloor uplift offshore SW Africa.

Acknowledgements

This study has been done within the framework of the priority program SAMPLE (South Atlantic Margin Processes and Links with onshore Evolution; SPP 1375), funded by the German Research Foundation (DFG; grant no. SCHE 674/5-3). We are grateful to Julia Autin for providing the thickness maps used in this study.

Furthermore we would like to thank the reviewers for their constructive comments which helped to improve the manuscript.

References

Airy GB (1855). On the computation of the effect of the Attraction of Mountain-masses, as disdurbing the apparent astronomical latitude of station in geodetic surveys. Philos. Trans. R. Soc. London 145, 101–104.

Allken V, Huismans RS, Thieulot C (2012) Factors controlling the mode of rift interaction in brittle-ductile coupled systems: A 3D numerical study. Geochem. Geophys. Geosyst. 13 (5), Q05010. doi:10.1029/2012GC004077

Austin JA, Uchupi E (1982) Continental oceanic crustal transition off southwest Africa. Am. Ass. Petroleum Geologist Bull., 66, 1328-1347.

Athy LF (1930) Density, Porosity, and Compaction of Sedimentary Basins. Am. Assoc. Pet. Geol. Bull. 14, 1–24.

Autin J, Scheck-Wenderoth M, Loegering MJ, Anka Z, Vallejo E, Rodriguez JF, Dominguez F, Marchal D, Reichert C, di Primio R, Götze HJ (2013) Colorado Basin 3D structure and

evolution, Argentine passive margin. Tectonophyiscs 604, 264-279 doi:10.1016/j.tecto.2013.05.019

Autin J, Scheck-Wenderoth M, Götze HJ, Reichert C, Marchal D (2015) Deep structure of the Argentine margin inferred from 3D gravity and temperature modelling, Colorado Basin. Tectonophysics. doi10.1016/j.tecto.2015.11.023

Bott MHP (1992) Passive margins and their subsidence. Journal of Geological Society 149, 805-812

Braun J, Guillocheau F, Robin C, Baby G, Jelsma H (2014) Rapid erosion of the Southern African Plateau as it climbs over a mantle supersell. J. Geophys. Res. Solid Earth 119:6093-6112. doi:10.1002/2014JB010998

Brown LF, Benson Jr JM, Brink GJ, Doherty S, Jollands A, Jungslager EHA, Keenan JHG, Muntingh A, van Wyk NJS (1995) Sequence stratigraphy in offshore South African divergent basins. An atlas on exploration for Cretaceous lowstand traps by Soeker (Pty) Ltd. AAPG, Studies in Geology 41

Brune S, Popov A, Sobolev SV (2013) Quantifying the thermo-mechanical impact of plume arrival on continental break-up. Tectoniphysics 604, 51-59. doi:10.1016/j.tecto.2013.02.009

Brune S (2014) Evolution of stress and fault patterns in oblique rift systems: 3-D numerical lithospheric-scale experiments from rift to breakup. Geochem. Geophys. Geosyst. 15, 3392-3415. doi:10.1002/2014GC005446

Brune S, Heine C, Pérez-Gussinyé M, Sobolev SV (2014) Rift migration explains continental margin asymmetry and crustal hyper extension. Nature commun.5:4014. doi:10.1038/ncomms5014.

Burov E, Guillou-Frottier L, d'Acremont E, Le Pourhiet L, Cloething S (2007) Plume head-lithosphere interactions near intrac-continental plate boundaries. Tectonophysics 343: 15-38. doi: 10.1016/j.tecto.2007.01.002

Burov E, Cloething S (2010) Plume-like upper mantle instabilities drive subdaction initiation. Geophys. Res. Letters 37:L03309. doi:10.1029/2009GL041535

Cobbold PR, Rossello EA, Roperch P, Arrigada C, Gomez LA, Lima C (2007) Distribution, timing, and causes of Andean deformation across South America. In: Ries AC, Butler RWH, Graham RH (Eds.), Deformation of the Continental Crust: The Legacy of Mike Coward. Geol. Soc. London, Spec. Publ., vol. 272, pp. 321-343.

Cohen, K.M., Finney, S.M., Gibbard, P.L., Fan, J.-X., 2013. The ICS International Chronostratigraphic Chart, Episodes 36 (3): 199-204

Colli L, Stotz I, Bunge HP, Smethurst M, Clark S, Iaffaldano G, Tassara A, Guillocheau F, Bianchi MC (2014). Rapid South Atlantic spreading changes and coeval vertical motion in surrounding continents: Evidence for temporal changes of pressure-driven upper mantle flow. Tectonics 32:1304–1321. doi:10.1002/2014TC003612

Demoulin A, Zarate M, Rabassa J (2005) Long-term landscape development: a persepctive from the southern Buenos Aires ranges of eaast central Argentina. Journal of South Am. Earth Sci. 19, 193-204. doi:10.1016/j.jsames.2004.12.001

Dominguez F, Marchal D, Sigismondi M, Espejón C, Vallejo E (2011) Caracterización de dominios estructuraled e influencia de estructuras preexistentes en hemigábenes de rift en el sector centro-norte de la Plataforma Continental Argentina. Actas XVIII Congreso Geológico Argentino.

Dupré S, Cletingh S, Bertotti G (2011) Structure of the Gabon Margin from integrated seismic reflection and gravity. Tectonophysics 506, 31-45. doi:10.1016/j.tecto.2011.04.009

Dressel I, Scheck-Wenderoth M, Cacace M, Lewerenz B, Götze HJ, Reichert C (2015) Reconstruction of the southwestern African continental margin by backward modeling. Mar. Pet. Geol. 67:544-555. doi:10.1016/j.marpetgeo.2015.06.006

Dressel I, Cacace M, Scheck-Wenderoth M (2016) Coupled thermo-mechanical 3D subsidence analysis along the SW African passive continental margin. Arab. J. Geosci. 9:385. doi: 10.1007/s12517-016-2407-9

Flament N, Gurnis M, Müller RD (2013) A review of observations and model of dynamic topography. Lithosphere. doi:10.1130/L245.1

Franke D, Neben S, Schreckenberger B, Schulze A, Stiller M, Krawczyk CM (2006) Crustal structure across the Colorado Basin, offshore Argentina. Geophysical Journal International 165, 850-864. doi:10.1111/j.1365-246X2006.02907.x

Franke D, Neben S, Ladage S, Schreckenberger B, Reichert C, Hinz K (2007) Margin segmentation and volcano-tectonic architecture along the volcanic margin off Argentine/Uruguay, South Atlantic. Marine Geology 244, 46-67. doi:10.1016/jmargeo.2007.06.009

Franke D, Ladage S, Schnabel M, Schreckenberger B, Reichert C, Hinz K (2010) Birth of a volcanic margin off Argentina, South Atlantic. Geochemistry Geophysics Geosystems 11 (2), 1-20. doi:10.1029/2009GC002715

Gladczenko TP, Skogseid J, Eldhom O (1997) South Atlantic volcanic margins. Journal of the Geol. Soc. London 154, 465-470

Gurnis M, Mitrovica JX, Ritsema J, van Heijst HJ (2000) Constraining mantle density strucutre using geological evidence of surface uplift rates: the case of the African superplume. Geochm. Geophy. Geosyst. 1 doi:10.1029/1999GC000045

Hartwig A, Anka Z, di Primio R (2012) Evidence of a widespread paleo-pockmarked field in the Orange Basin: An indication of an early Eocene massive fluid escape event offshore South Africa. Mar. Geol. 332-334:222–234. doi:10.1016/j.margeo.2012.07.012

Hinz K, Neben S, Schreckenberger B, Roeser HA, Block M, Goncalves de Souza H (1999) The Argentine continental margin north of 48°S: sedimentary successions, volcanic activity during breakup. Mar. Pet. Geol. 16:1-25.

Hirsch KK, Scheck-Wenderoth M, Paton DA, Bauer K. (2007) Crustal structure beneath the Orange Basin, South Africa. South African J. Geol. 110:249–260. doi:10.2113/gssajg.110.2-3.249

Hirsch KK, Bauer K, Scheck-Wenderoth M (2009) Deep structure of the western South African passive margin - Results of a combined approach of seismic, gravity and isostatic investigations. Tectonophysics 470:57–70. doi:10.1016/j.tecto.2008.04.028

Hirsch KK, Scheck-Wenderoth M, van Wees JD, Kuhlmann G, Paton D A (2010). Tectonic subsidence history and thermal evolution of the Orange Basin. Mar. Pet. Geol. 27:565–584. doi:10.1016/j.marpetgeo.2009.06.009

Huismans R, Beaumont C (2011): Depth-dependent extension, two-stage breakup and cratonic underplating at rifted margins. Nature 473:74-78. doi:10.1038/nature09988

Huismans R, Beaumont C (2014) Rifted continental margins: the case for depth-dependent extension. Earth and Planet. Sci. Lett. 407:148-162. doi:10.1016/j.epsl.2014.09.032

IOC, IHO, BODC (2003). Centenary Edition of the GEBCO Digital Atlas, published on CD-ROM on behalf of the Intergovernmental Oceanographic Commission and the International Hydrographic Organization as part of the General Bathymetric Chart of the Ocean; British Oceanographic Data Centre, Liverpool

Japsen P, Chalmers JA, Green PF, Bonow JM (2012) Elevated, passive continental margins: Not rift shoulders, but expressions of episodic, post-rift burial and exhumation. Glob. Planet. Change 90-91:73–86. doi:10.1016/j.gloplacha.2011.05.004

Jungslager EHA (1999). Petroleum habitats of the Atlantic margin of South Africa, in: Cameron, N.R., Bate, R.H., Clure, V.S. (Eds.), The oil and gas habitats of the South Atlantic. Geol. Soc. London, Spec. Publ. 153, 153–168. doi:10.1144/GSL.SP.1999.153.01.10

Katz BJ, Mello MR (2000) Petroleum Systems of South Atlantic marginal basins - an overview. in MR Mello and BJ Katz (Eds), Petroleum systems of South Atlantic margins: AAPG Memoir 73, 1-13

Koopmann H, Brune S, Franke D, Breuer S (2014) Linking rift propagation barriers to excess magmatism at volcanic rifted margins. Geology 42 (12), 1071-1074. doi:10.1130/G36085

Kuhlmann G, Adams S, Campher C, van der Spy D, di Primio R, Horsfield B (2010) Passive margin evolution and its controls on natural gas leakage in the southern Orange Basin, blocks 3/4, offshore South Africa. Mar. Pet. Geol. 27, 973-992. doi:10.1016/j.marpetgeo.2010.01.010

Kuhlmann G, Adams S, Anka Z, Campher C, di Primio R, Horsfield B (2011) 3D Petroleum Systems Modelling Within a Passive Margin Setting, Orange Basin, Blocks 3/4, Offshore South Africa - Implications for Gas Generation, Migration and Leakage. South African J. Geol. 114:387–414. doi:10.2113/gssajg.114.3-4.387

Le Pourhiet L, Huet B, May DA, Labrousse L, Jolivet L (2012) Kinematic interpretation of the 3D shapes of metamorphic core complexes. Geochem. Geophys. Geosyst. 13 (9), Q09002. doi:10.1019/2012GC004271

Liao J, Gerya T (2015) From continental rifting to seafloor spreading: Insight from 3D thermo-mechanical modeling. Gondwana Res. 28 (4), 1329-1343. doi:10.1016(j.gr.2014.11.004

Loegering M, Anka Z, Autin J, di Primio R, Marchal D, Rodiguez JF, Franke D, Vallejo E (2013) Tectonic evolution of the Colorado Basin, offshore Argentina, inferred from seismo-stratigraphy and depositional rates analysis. Tectonphysics 604:245-263. doi:10.1016/j.tecto.2013.02.008

Lithgow-Bertelloni C, Silver P (1998) Dynamic topography plate driving forces and the African superswell. Nature 395, 345-348

Marcano G, Anka Z, di Primio R (2013) Major controlling factors on hydrocarbon generation and leakage in South Atlantic conjugate margins: A comparative study of Colorado, Orange, Campos, and Lower Congo basins. Tectonophysics 604, 172-190. doi:10.1016/j.tecto.2013.02.004

Maystrenko YP, Scheck-Wenderoth M, Hartwig A, Anka Z, Watts AB, Hirsch KK, Fishwick S (2013) Structural features of the Southwest African continental margin according to results of lithosphere-scale 3D gravity and thermal modelling. Tectonophysics 604:104–121. doi:10.1016/j.tecto.2013.04.014

McKenzie D (1978) Some remarks on the development of sedimentary basins. Earth Planet. Sci. Lett. 40:25–32

Moucha R, Forte AM (2011) Changes in African topography driven by mantle convection. Nat. Geosci. 4:707–712. doi:10.1038/ngeo1235

Nyblade A, Robinson S (1994) The African superswell. Geophys. Res. Lett. 21, 765–768.

Paton DA, di Primio R, Kuhlmann G, van der Spuy D, Horsfield B (2007) Insights into the Petroleum System Evolution of the southern Orange Basin, South Africa. South African J. Geol. 110:261-274. doi: 10.2113/gssajk.110.2-3.261

Rabinowitz PD, Labrecque J (1979) The Mesozoic South Atlantic Ocean and evolution of its continental marings. Journal of Geophy. Res. 84 (B11), 5973-6002

Ritsema J, van Heijst HJ, Woodhouse JH (1999) Complex shear wave velocity strucutre imaged beneth Africa and Iceland. Science 286, 1925-1928

Rouby D, Braun J, Robin C, Dauteuil O, Deschamps F (2013) Long-term stratigraphic evolution of Atlantic-type passive margins: A numerial approach of interactions between surface processes, flexural isostasy and 3D thermal subsidence. Tectonophysics 604:83-103. doi:10.1016/j.tecto.2013.02.003

Sachse VF, Strozyk F, Anka Z, Rodriguez JF, di Primio R (2015) The tectono-stratigraphic evolution of the Austral Basin and adjacent areas against the background of Andean tectonics, southern Argentina, South America. Basin Research, 1-21. doi:10.1111/bre.12118

Scheck M, Bayer U, Lewerenz B (2003) Salt redistribution during extension and inversion inferred from 3D backstripping. Tectonophysics 373, 55–73. doi:10.1016/S0040-1951(03)00283-X

Schnabel M, Franke D, Engels M, Hinz K, Neben S, Damm V, Grassmann S, Pelliza H, Dos Santos PR (2008) The structure of the lower crust at the Argentine continental margin, South Atlantic at 44°S. Tectonophysics 454, 14-22. doi:10.1016/j.tecto.2008.01.019

Séranne M, Anka Z (2005) South Atlantic continental margins of Africa: a comparison of the tectonic vs climate interplay on the evolution of equatorial west Africa and SW Africa margins. J. African Earth Sci. 43:283–300. doi:10.1016/j.jafrearsci.2005.07.010

Sibuet JC, Hay WW, Prunier A, Montadert L, Hinz K, Fritsch J (1984) Early evolution of the South Atlantic Ocean: role of rifting episode. DSDP Volume LXXV, 483-508. doi:102973/dsdp.proc.75.1984

Stewart J, Watts AB, Bagguley JG (2000) Three-dimensional subsidence analysis and gravity modelling of the continental margin onshore Namibia. Geophys. J. Int. 141:724–746

Thybo H, Artemieva IM (2013) Moho and magmatic underplating in continental lithosphere. Tectonophysics 609:605-619. doi:10.1016/j.tecto.2013.05.032

Torsvik TH, Rousse S, Labails C, Smethurst MA (2009). A new scheme for the opening of the South Atlantic Ocean and the dissection of an Aptian salt basin. Geophys. J. Int. 177, 1315–1333. doi:10.1111/j.1365-246X.2009.04137.x

Trumbull RB, Reid DL, de Beer C, van Acken D, Romer RL (2007) Magmatism and continental breakup at the west margin of southern Africa: A geochemical comparison of dolerite dikes from northwestenr Namibia and the Western Cape. South African J. Geol. 110, 477–502. doi:10.2113/gssajg.110.2-3.477

Winterbourne J, White N, Crosby A (2014) Accurate measurements of residual topography from the oceanic realm. Tectonics 33, 982-1015. doi:10.1002/2013TC003372

Figures

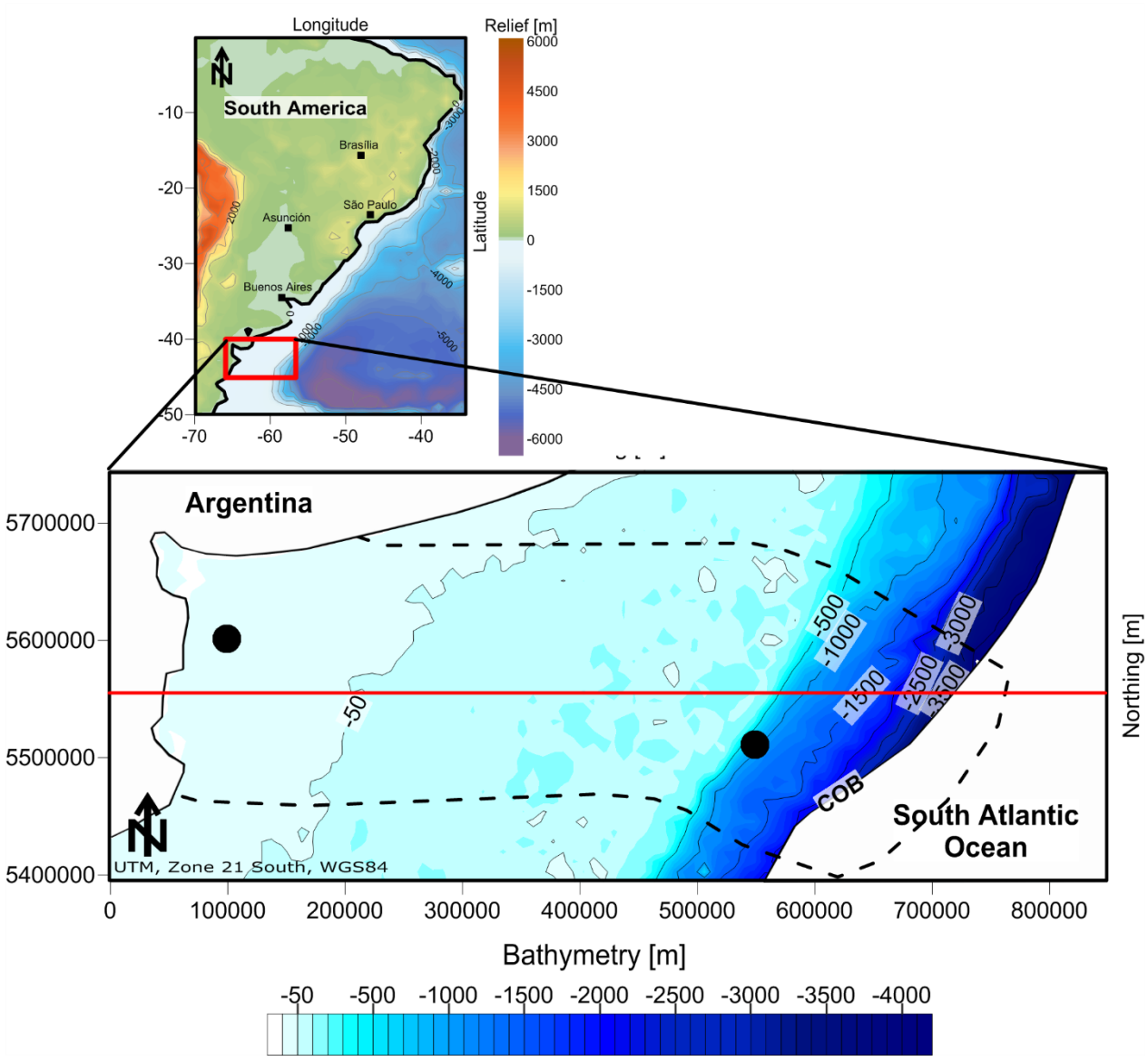

Figure 1: Map of the research area with overview of the location in the eastern South America (bathymetry after IOC, IHO and BODC, 2003). The contour of the Colorado Basin is marked by the black dashed line. The black dots mark the location of synthetic boreholes used for Figure 4 and 10 as these locations represent the areas of the thickest sediment deposition whereas the red solid line show the location of the cross-section shown in Figure 5.

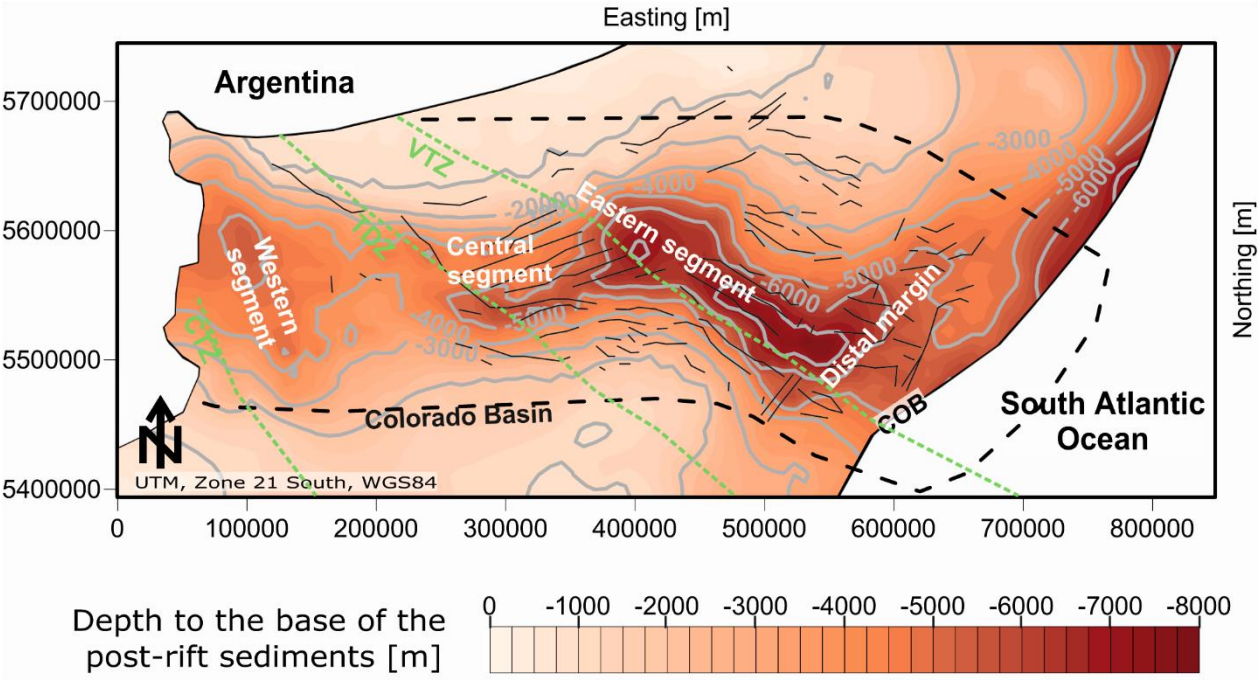

Figure 2: Depth to the base of the post-rift sediments (Autin et al., 2013) indicating a NW-SE oriented depocentre in the western segment and a rather NE-SW oriented depocentre in the distal margin. The contour of the Colorado Basin is marked by the black dashed line and segmented into four major segments according to Autin et al. (2015). Major faults of the pre-rift basement are highlighted by the solid black lines (Autin et al., 2015) and transfer zones by grey dashed lines (CTZ: Colorado Transfer Zone; TDZ: Tona Deformation Zone; VTZ: Ventana Transfer Zone; Franke et al. 2006; Dominguez et al., 2011).

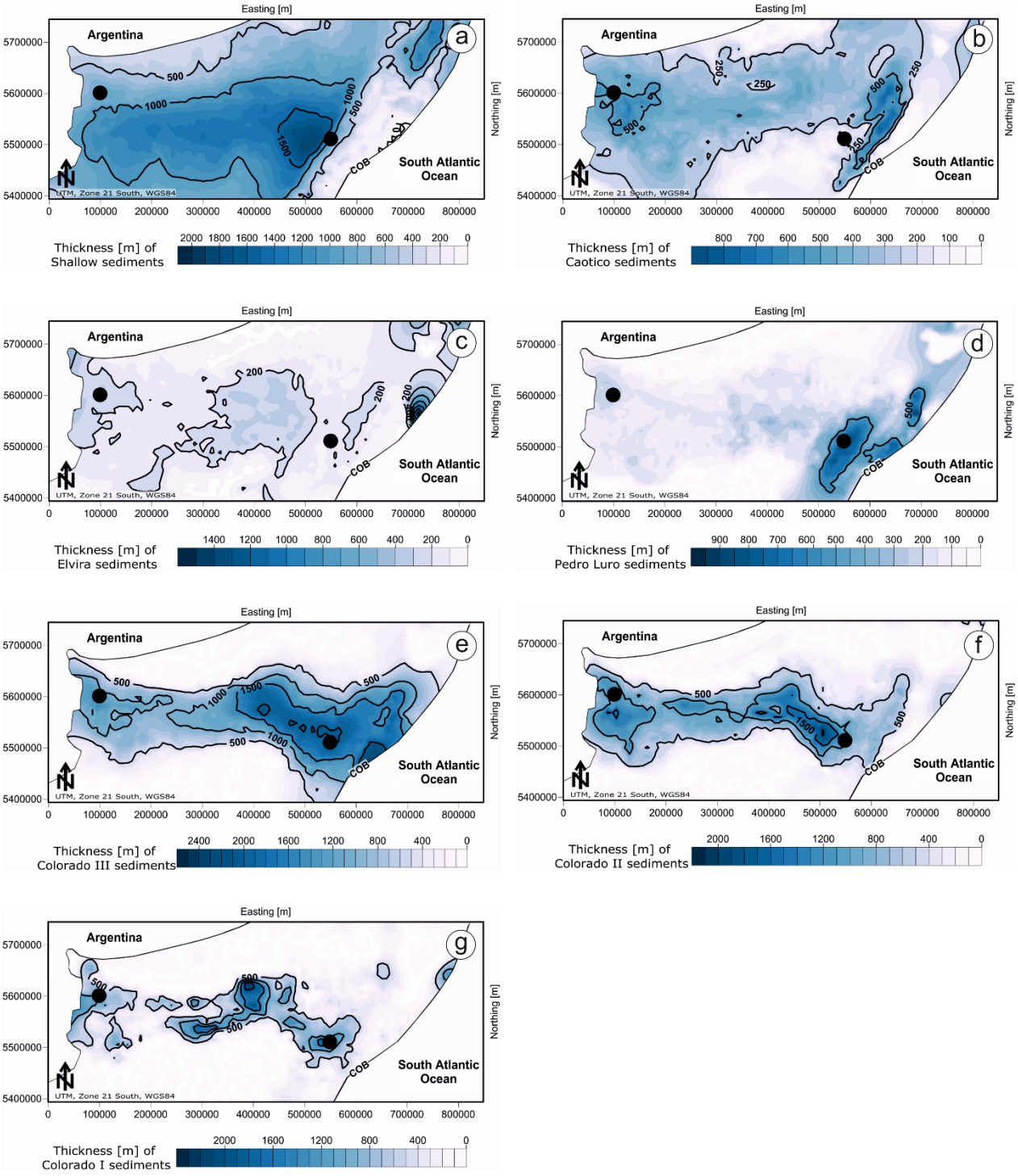

Figure 3: Thickness maps indicating the two major orientations of deposition. (a) Shallow sediments (0 – 25 Ma). (b) Caotico sediments (25 – 40 Ma). (c) Elvira sediments (40 – 55 Ma). (d) Pedro Luro sediments (55 – 70 Ma). (e) Colorado III sediments (70 – 90 Ma). (f) Colorado II

sediments (90 – 98 Ma). (g) Colorado I (98 – 125 Ma). The black dots mark the area of synthetic wells shown in Figure 4 and 6. Modified after Autin et al. (2013, 2015).

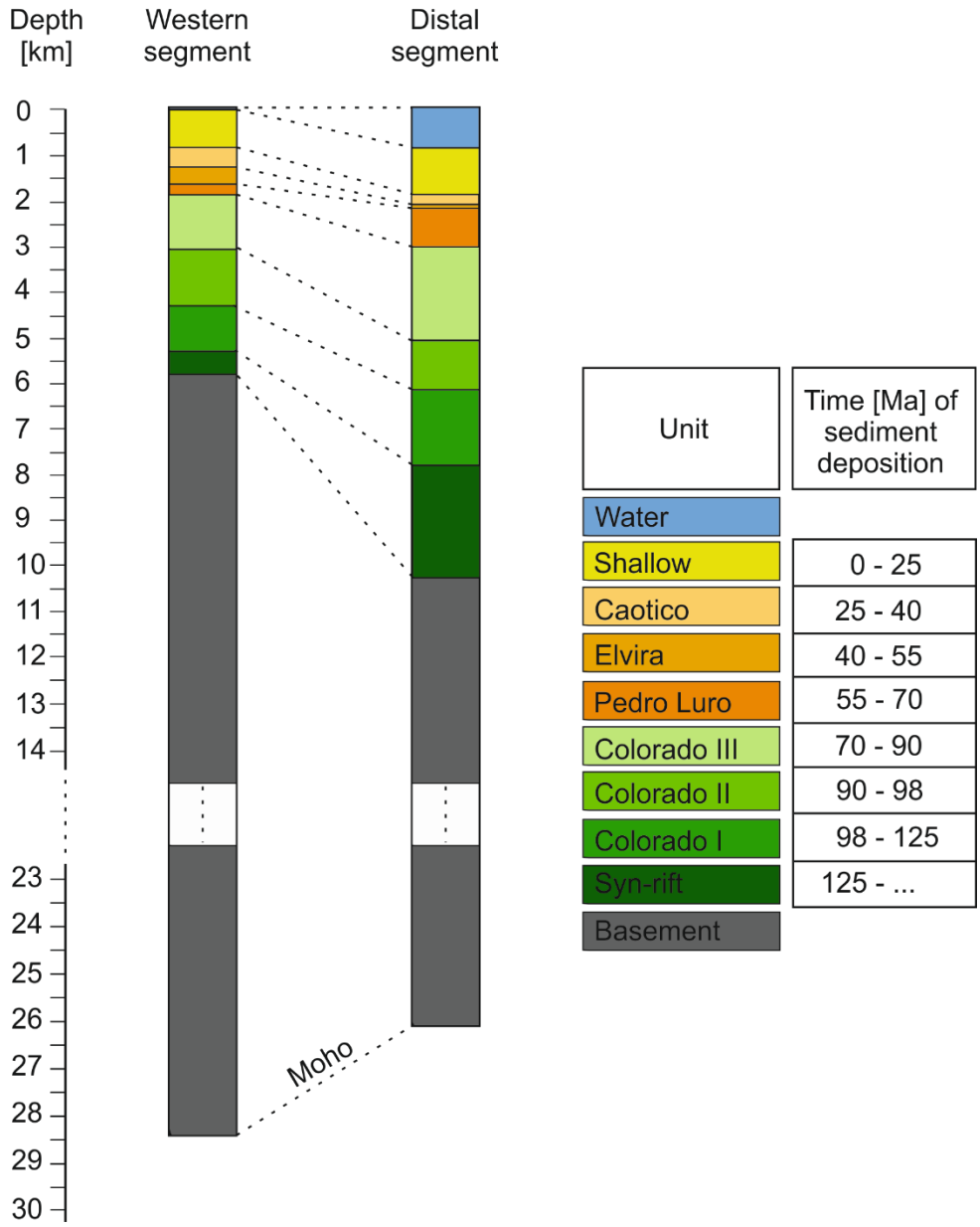

Figure 4: Stratigraphy of two synthetic wells in each of the major depocentres. See Figure 1 or 3 for the location. Information of thicknesses are taken from Autin et al. (2013, 2015).

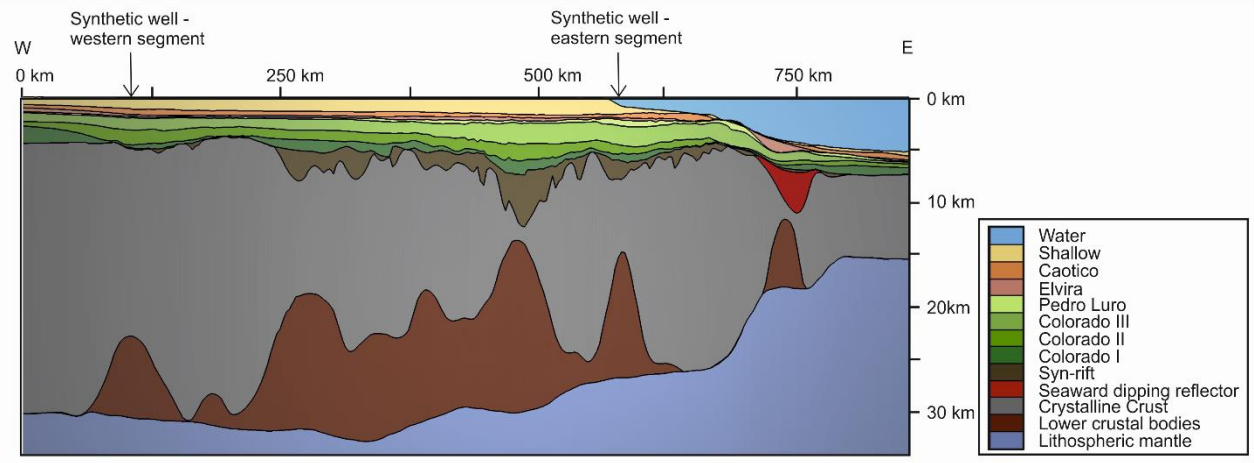

Figure 5: West-East profile across the centre of the Colorado Basin indicating a heterogeneous crustal configuration as well as the syn-rift and post-rift units. The location of the synthetic wells is shown by the black arrows on top of the profile; however, their location is about 40 km further to the north (western segment) and to the south (eastern segment), respectively. See Figure 1 for profile location. Information of thicknesses are taken from Autin et al. (2013, 2015).

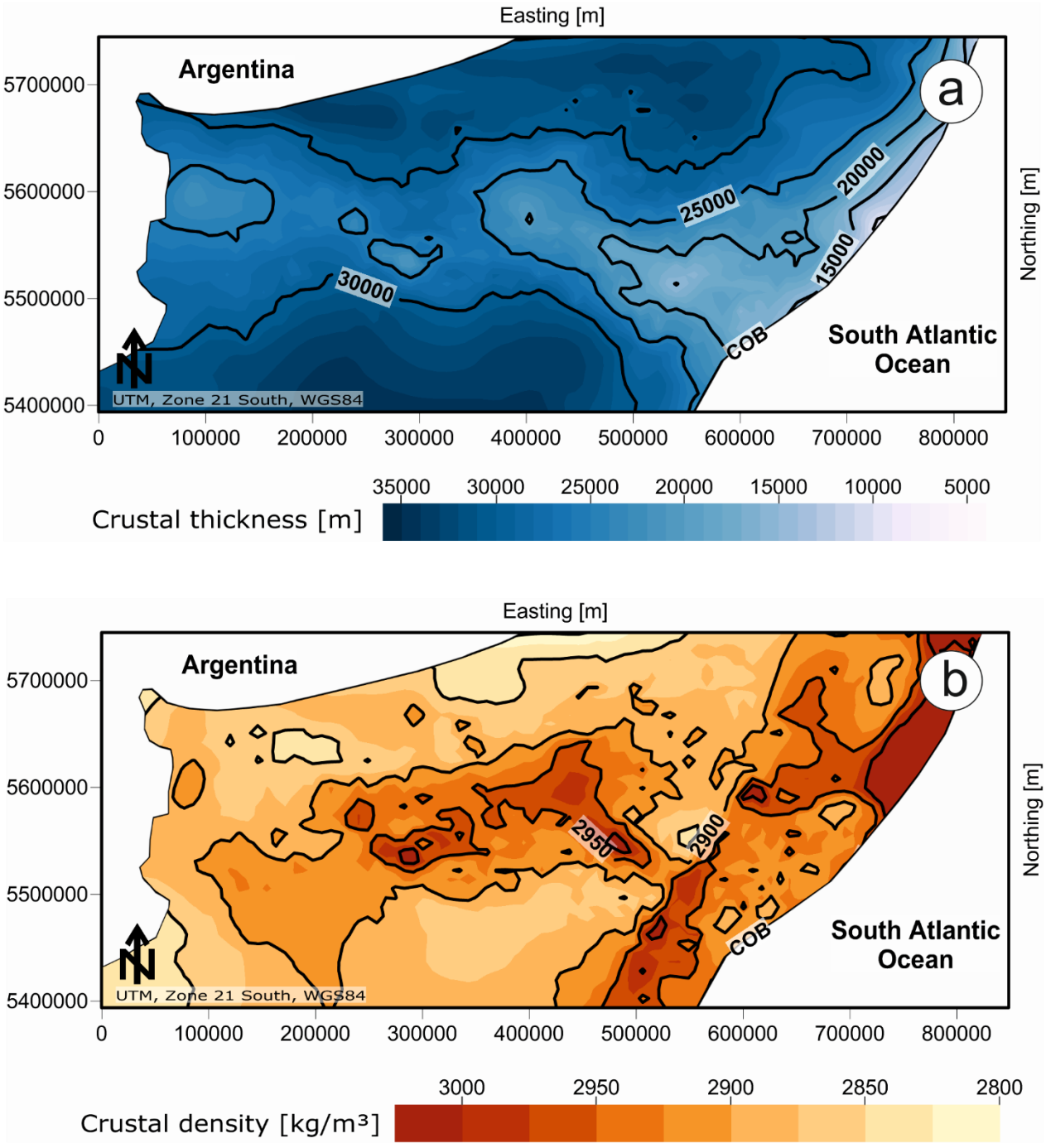

Figure 6: (a) Thickness of the present-day crust including SDRs, crystalline crustal domain and LCBs. (b) Laterally varying density of the crystalline crust. Areas of SDRs and LCBs are characterized by higher densities.

Table 1: Names, prevailing lithologies, ages, as well as physical properties used in the backward modelling approach. Names, prevailing lithologies and ages are taken from Autin et al. (2013) and references therein. However, the ages are modified after the time scale by Cohen et al. (2013). Physical properties are assigned to individual geological units according to the prevailing lithologies. Values for the physical properties were taken from Autin et al. (2015), Dressel et al. (2015), Sclater and Christie (1980). Density for the crust is laterally varying. For this reason it was calculated separately (see chapter 2 and Figure 6).

Name of individual units	Prevailing lithology used in this study	Ages of the unit [Ma]	Maxtrix Density [kg/m³]	Initial porosity	compaction factor
Seawater		0	1030	1	0
Shallow	Siltsones/Sandstones/gravels/gypsum/marls/loes/ pyroclastics	0-25	2720	0.63	0.77
Caotico	Gypsum/shales/sandstones/glauconitic sandstones/basalt/tuffs	25-40	2640	0.56	0.4
Elvira		40-55	2640	0.52	0.4
Pedro Luro	Shales/limestones/conglomerates/tuffs/basalts	55-70	2680	0.5	0.35
Colorado III	Continental clastics with marine shales	70-90	2600	0.5	0.35
Colorado II		90-98	2550	0.48	0.3
Colorado I	Continental to marine sandstones and conglomerates	98-125	2550	0.45	0.3
Synrift	Shales/sandstone/andesite and pyroclastic extrusion		2670	0.4	0.2
Crust (including SDR and LCB)			2700-3000		
Lithospehric mantle			3300		

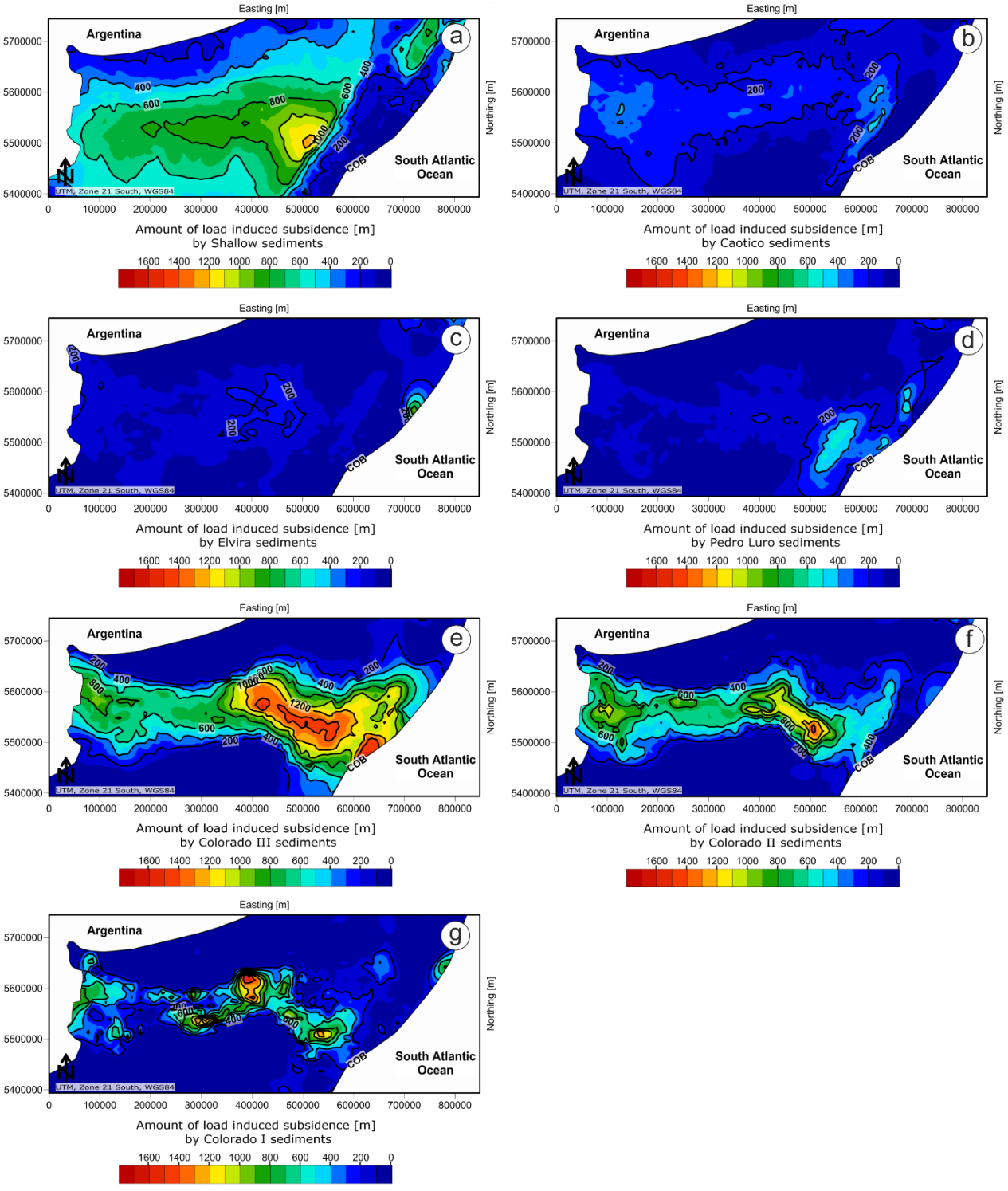

Figure 7: Amount of load induced subsidence for each of the post-rift phases. (a) Amount of load induced subsidence from 25 to 0 Ma. (b) Amount of load induced subsidence from 40 to 25 Ma. (c) Amount of load induced subsidence from 55 to 40 Ma. (d) Amount of load induced

subsidence from 70 to 55 Ma. (e) Amount of load induced subsidence from 90 to 70 Ma. (f) Amount of load induced subsidence from 98 to 90 Ma. (g) Amount of load induced subsidence from 125 to 98 Ma.

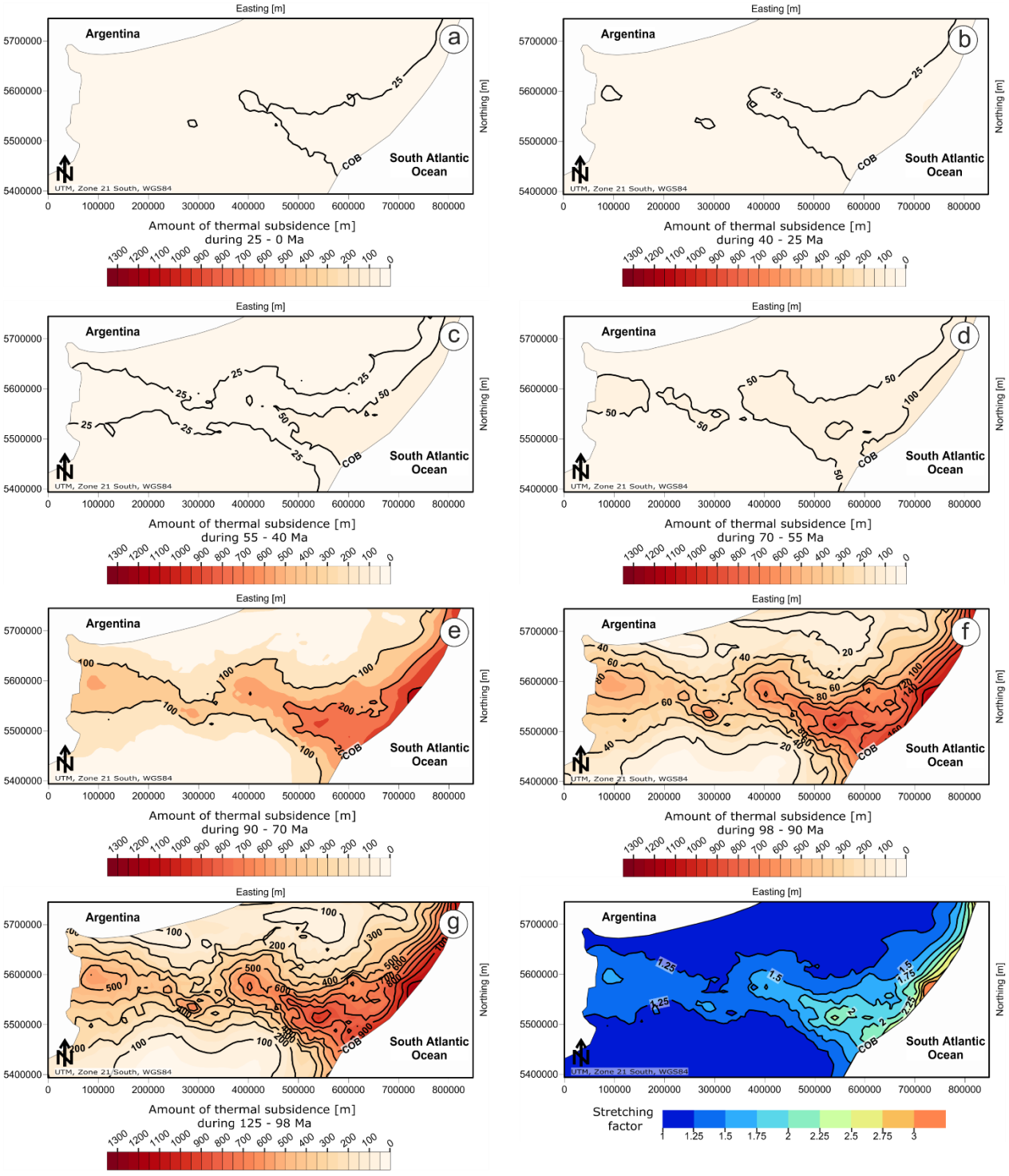

Figure 8: Amount of thermal subsidence for each of the post-rift phases. (a) Amount of thermal subsidence from 0 to 25 Ma. (b) Amount of thermal subsidence from 25 to 40 Ma. (c) Amount of thermal subsidence from 40 to 55 Ma. (d) Amount of thermal subsidence from 55 to 70 Ma. (e) Amount of thermal subsidence from 70 to 90 Ma. (f) Amount of thermal subsidence from 90 to

98 Ma. (g) Amount of thermal subsidence from 98 to 125 Ma. (h) The map illustrates the distribution of the stretching factor β. β is the result of the ratio between initial crustal thickness of 35,000 m and the present-day crustal thickness.

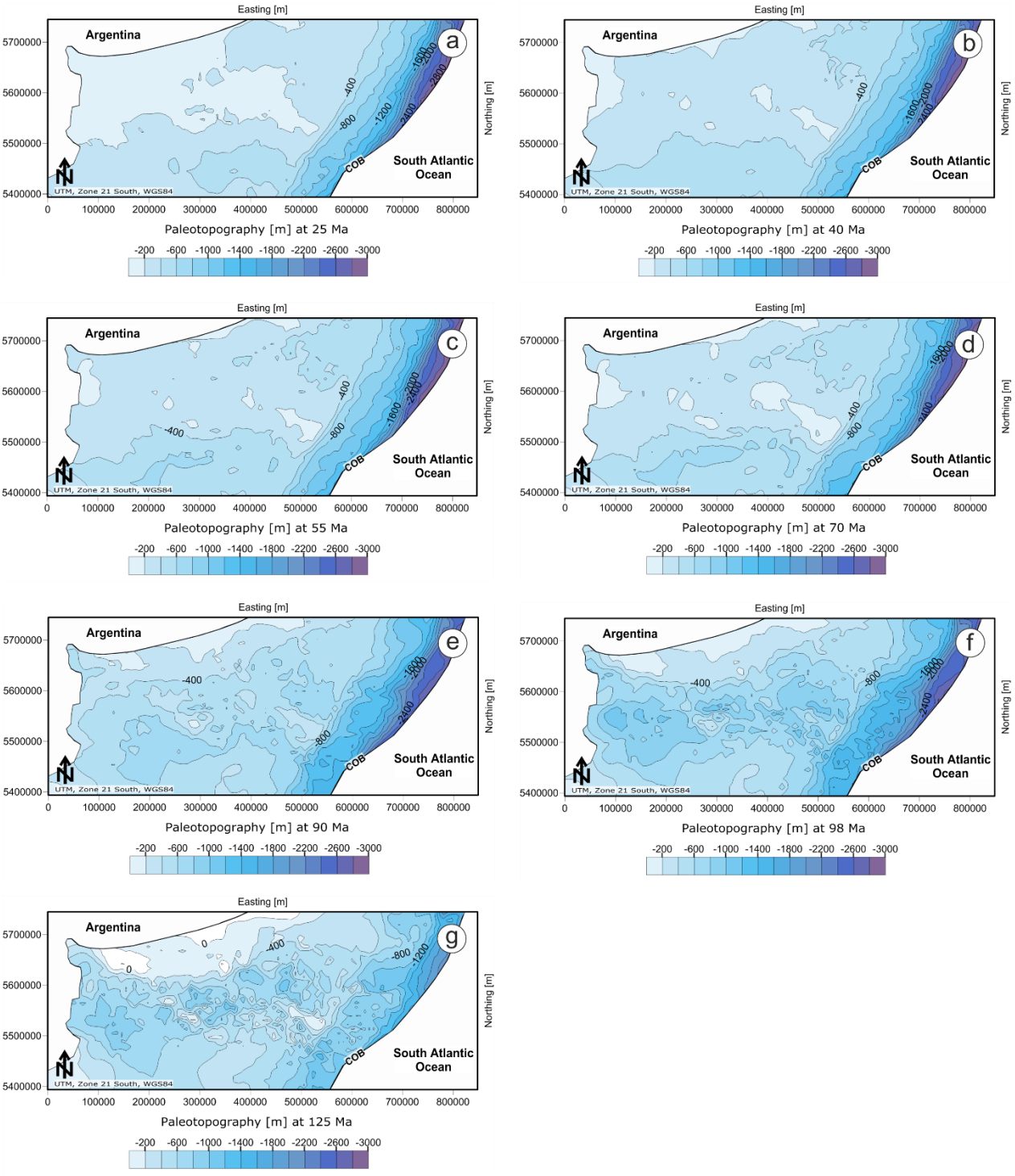

Figure 9: Paleobathymetries for seven times during the post-rift phase according to the model resolution. The maps are the result of the backward modelling approach assuming Airy isostasy and decompaction as well as thermal subsidence. (a) Paleobathymetry at the end of the Caotico unit (25 Ma). (b) Paleobathymetry at the end of the Elvira unit (40 Ma). (c) Paleobathymetry at the end of the Pedro Luro unit (55 Ma). (d) Paleobathymetry at the end of the Colorado III unit (70 Ma). (e) Paleobathymetry at the end of the Colorado II unit (90 Ma). (f) Paleobathymetry at the end of the Colorado I unit (98 Ma). (g) Paleobathymetry at the end of the Synrift unit (125 Ma).

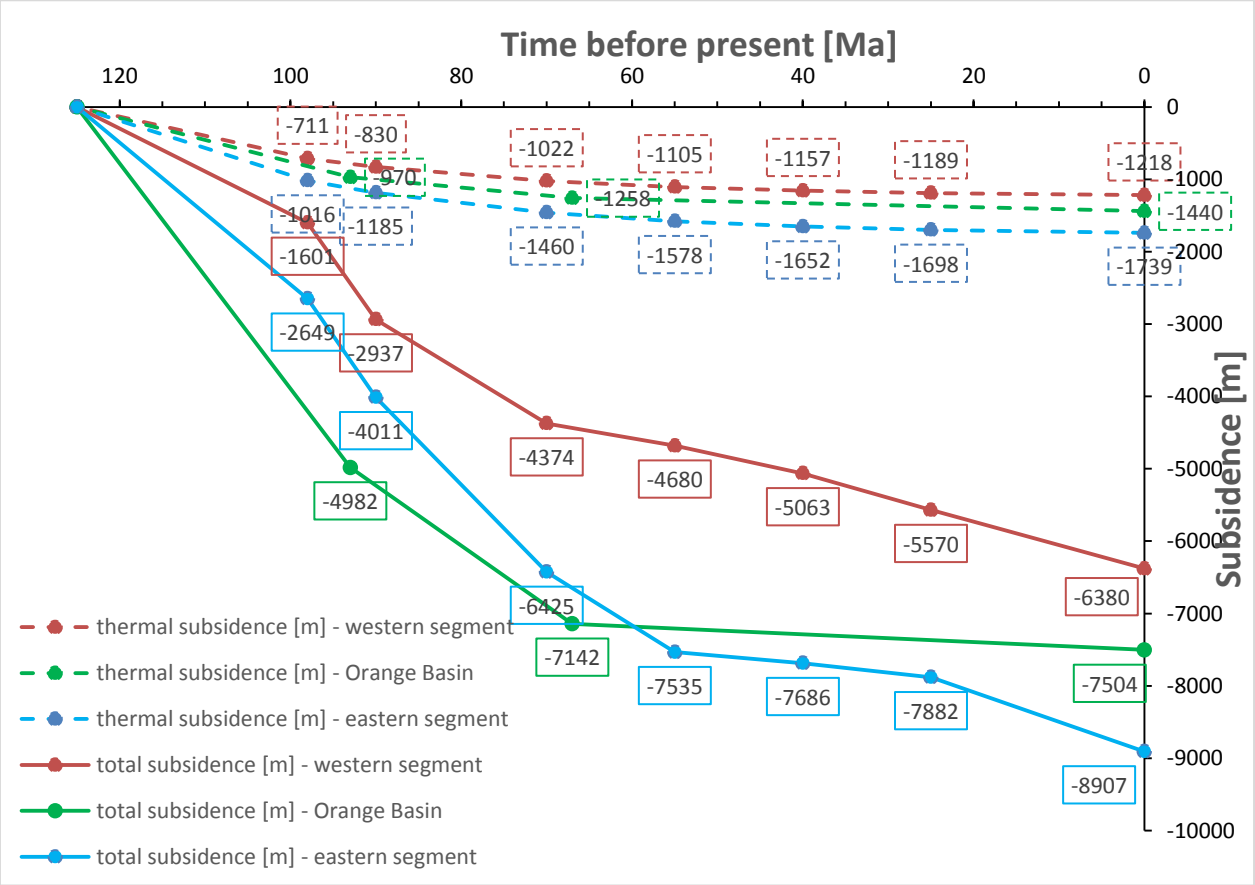

Figure 10: Subsidence curves for two synthetic wells in the eastern and western segment, respectively (orange and blue curve) as well as the subsidence curves for a synthetic well in the

Orange Basin (green curve, after Dressel et al., 2015). See Figure 1 for location. Solid curves show the thermal subsidence (β=1.73 for western segment; β=2.0 for Orange Basin; β=2.52 for eastern segment) while the dashed curves indicated the total subsidence; i.e. the sum of the thermal subsidence and the load induced subsidence. The amount of the latter is characterized by the space between the respective solid and the dashed curves.